Materials Science and Engineering A366 (2004) 104–113

MATERIALS SCIENCE & ENGINEERING A

www.elsevier.com/locate/msea

A synchrotron study of residual stresses in a Al6022 deep drawn cup

Thomas Gnaeupel-Herold [a,b,*], Henry J. Prask [b], Richard J. Fields [c], Timothy J. Foecke [c], Z. Cedric Xia [d], Ulrich Lienert [e]

[a] *Department of Materials and Nuclear Engineering, University of Maryland, College Park, MD 20742-2115, USA*
[b] *National Institute of Standards and Technology, Center for Neutron Research, Gaithersburg, MD 20899, USA*
[c] *National Institute of Standards and Technology, Metallurgy Division, Gaithersburg, MD 20899, USA*
[d] *FORD Scientific Research Laboratory, Dearborn, MI 48121, USA*
[e] *Advanced Photon Source, Argonne National Laboratory, Argonne, IL 60439-4815, USA*

Received 8 March 2003; received in revised form 28 August 2003

Abstract

Fueled by pressures to reduce scrap and tooling costs, the modeling and prediction of springback has become a major focus of interest in sheet metal forming. Finite element codes and packages are being developed or improved but face the demand for higher predictive accuracy which, in turn, requires accurate property data and a more complete understanding of the stresses that are responsible for the elastic part of the springback. In order to provide experimental data for these calculations, synchrotron X-ray diffraction measurements were carried out in order to determine the through-thickness distribution of axial and tangential residual stresses in an Al6022 deep drawn cup. The technique is able to provide true spatial resolutions of 0.05 mm for a strain measurement on a cup with 0.92 mm wall thickness. It is found that both axial and tangential stresses exhibit non-linear gradients through thickness and both exhibit a pronounced dependency on the axial position. The springback measured on a split ring cut from the cup agrees within 3% accuracy with the value predicted from the average of measured through-thickness stresses.

Keywords: Springback; Sheet metal forming; Stress; Synchrotron

1. Introduction

The stamping of sheet metal induces complex deformations, which in different regions of the sheet metal can have vastly different accumulated plastic strains. Upon unloading by removing the die, springback occurs which changes the dimensions of the part. Springback is caused by non-uniform residual stresses through the thickness of the sheet metal that create a bending moment which causes a distortion of the part upon unloading. Springback strains are almost completely elastic; non-linear recovery strains are usually small but, in extreme cases, they can amount up to 10% of the total recovery [1]. The accurate prediction of the springback is of major interest for small part tolerances and to avoid a costly redesign of the stamping tool. In the past a number of studies have looked into ways of reducing springback, particularly the role of pre-straining, blankholder force and yield strength. Still, even in this case springback cannot be disregarded completely but it can be reduced which allows a more accurate prediction with smaller absolute tolerances (not necessarily relative tolerances). Experimental data of springback stresses are scarce in the available literature; instead, most publications deal with the modeling aspect of the problem, thus highlighting the need for data that can benchmark the model predictions.

The stresses, which are generally bi-axial, are created when sheet metal is subjected to bending operations during which locations with different thickness coordinates undergo different strain paths, thus producing stress differentials across sheet metal thickness and leading to bending moment upon tool removal. An accurate modeling of springback thus requires accurate prediction of pointwise stresses throughout.

In an attempt to simplify the problem, various studies have dealt with symmetric, generic shapes among which circular cups have received the most attention [3–7] as a promising way to characterize a material's springback properties in a quick and consistent way. For a standardizable test, it

* Corresponding author. Tel.: +1-301-975-5380; fax: +1-301-921-9847.
E-mail address: tg-h@nist.gov (T. Gnaeupel-Herold).

0921-5093/$ – see front matter © 2003 Elsevier B.V. All rights reserved.
doi:10.1016/j.msea.2003.08.059

is desirable that it be fairly easy, repeatable and in the case of this particular need, have a large springback component that can be easily measured. A test that has received considerable attention consists of a ring sample taken from the sidewall of a flat bottom, deep drawn cup. The main advantage of such a simple geometry is that the springback can be measured very easily by cutting off rings and subsequently splitting them. Using this operation, the through-thickness stress change can be calculated very easily, thus providing a means to follow stress variations induced by changing certain stamping parameters such as ironing [2,6].

For this to be useful also for non-generic parts with more complicated strain paths the successful simulation of the springback must be based on an accurate prediction of the depth distribution of stresses. However, because of the small thicknesses involved a pointwise stress measurement to validate the models has been very difficult and there are few studies that provide even approximate experimental results.

Saito and Shimahashi [3] employed Sachs' boring method on a mild steel deep drawn cup and obtained both axial and tangential stresses that indicate a highly non-linear gradient of stresses both in the axial and radial direction. Their results are based on data from a single strain gage with no distinction between strain gage location and the original rolling direction (RD) of the blank. Because this method of stress depth profiling is essentially based on layer removal the results depend on the sequence of the removal, i.e. if layers are removed from the inner or the outer surface. The reconstruction of the undisturbed stress state was not possible because one prerequisite of the boring-out theory, namely that the stresses are constant along the length, was clearly not applicable. Danckert [2] used a variation of layer removal together with X-ray diffraction for monitoring the stress changes. Yuying et al. [5] used a similar method of layer removal together with X-ray diffraction on stainless steel cups having varying degrees of strain-induced martensite. Their findings revealed vastly different through-thickness tangential stresses depending on the content of induced martensite.

In contrast to the layer-removal methods, diffraction techniques offer the only possibility for mapping stress variations through the thickness, circumferentially, and axially. For example, early advances in neutron diffraction instrumentation in combination with a high neutron flux made it possible to achieve spatial resolutions in the sub-millimeter range, thus enabling the first non-destructive measurements on $\approx$1 mm thick cups by Lange and Bruckner [4]. They confirmed that the through-thickness stress gradients in a 1 mm thick brass cup are non-linear but concluded that higher spatial resolutions were required to elucidate the stress distribution with sufficient detail.

In order to avoid the aforementioned difficulties in destructive stress determination there is no alternative to diffraction methods, either as neutron or as synchrotron diffraction. In practice, even tighter restrictions are imposed by sheet metal thicknesses of $\leq$1 mm where neutron diffraction reaches the limit of its capability. Synchrotron diffraction is basically the only method capable both of penetrating 1 mm of aluminum and providing spatial resolutions $<$0.1 mm. In this paper we describe the results of such measurements on an intact and a split ring cut from an Al6022 cup. The investigation included measurements of axial and tangential stresses on different axial locations and around the circumference.

It is conceivable that the stress state in the initial blank as induced by rolling would have some effect on the springback of the rings. However, any pre-existing stresses in the blank have a zero bending moment (or the blanks would not be flat), thus they cannot add to the springback. More important are the initial plastic strains due to rolling. These plastic strains tend to be present as a gradient symmetrical to the mid-plane of the sheet and, especially for thicker blanks, the strains can be substantial near the sheet surfaces. As a result, the initial yield stress of the blank may not be uniform through the thickness, thus possibly affecting the stress differential after forming. In an experiment described in [8] through-thickness stress measurements were performed on cup rings made of as-received and stress-relieved AISI-1010 blanks. It was found that the through-thickness residual stresses in both cups were virtually identical. When comparing the blank thickness of 3 mm used in [8] to the sheet thickness used here (0.92 mm) we can assume that the effect of the initial plastic strain from rolling both on the residual stresses due to forming and on the springback is small.

2. Experimental

A ring with 110 mm in diameter, 15.0 mm in height and 0.92 mm wall thickness was cut by EDM from the center section of a deep-drawn cup (Fig. 1a and b). Except for the height ($\pm$0.1 mm), the dimensions are approximate due to the cup being slightly conical and because of thickness variations of about 0.1 mm due to flow anisotropy. The procedure was then repeated on a second cup made under the same forming conditions and the ring was split open. No pre-strain was applied. As shown by the results in Table 1, the level of control over the conditions of the deep drawing is such that the springback values of four different rings are within 3% of their average, thus justifying the comparison of stresses in different rings.

Table 1
Ring openings and radii of rings made under identical conditions as the ones investigated here

Specimen no.	Opening $2y$ (mm)	Radius of the split ring R (mm)	Calculated radius R of the split ring (calculated from measured stresses) (mm)
6022-9	80.2	68.5	70.8
6022-10	82.5	68.9	
6022-11	79.25	68.32	
6022-12	84.33	69.25	

The value in the last column was calculated from the through-thickness stress profiles.

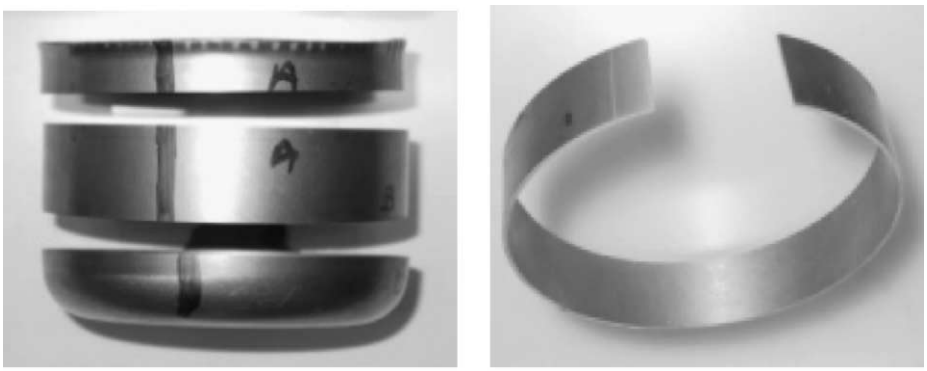

(a) (b)

Fig. 1. Sectioned cup (a) and split ring (b).

On the intact ring, through thickness measurements were performed on two axial locations, one in the middle of the ring, the other 5 mm towards the cup bottom. On the split ring, measurements were performed in the middle, 4.5 mm towards the top, and 5 mm towards the bottom. The measurement locations around the circumference (intact: 0, 180° = RD, split: 90° = TD, 180° = RD) were set with respect to the rolling direction of the original blank material. A sketch is shown in Fig. 2. Because of the tight restrictions of the beamtime at the synchrotron it was not possible to measure more locations.

In sheet metal forming one has to deal with plane stress states for which the normal stress ("radial" in Fig. 2) can be safely set to zero everywhere. This allows the use of a scheme in which the unknowns tangential stress and axial stress are obtained from three measured strains in the axial, tangential and radial directions [9,10]. For this method an estimate for the unstressed d-spacing is sufficient [10].

Residual stress measurements were performed at the 1IDB beamline at the Advanced Photon Source at the Argonne National Lab. Because the basic principles of diffraction residual stress analysis are well known [10], only the specifics of this measurement will be described. Fig. 3 shows a schematic of the experimental setup.

Despite the relatively low photon energy of 20 keV the high intensity of the primary beam allowed the use of the Al(4 2 2) sample reflection, thus increasing the Bragg angle to approx. $2\theta \approx 44°$. This choice decreases the notorious "diamond" distortion of the sampling volume and maintains the nominal spatial resolution. In order to minimize the intrinsic blurring of the shape of the sampling volume due to cold-work induced peak broadening a Si(1 1 1) analyzer crystal was used to restrict the acceptance angle of the detector. This measure removed the instrumental line broadening. A typical peak profile is shown in Fig. 4. The counting time was chosen such that the typical uncertainty of the peak position was $\leq 5 \times 10^{-5}$.

Despite the small sampling volume ($\approx 0.003\,\text{mm}^3$), and the fact that aluminum alloys virtually always contain large grains, for the same orientation but different locations the intensity fluctuations of the reflected peak were within 62% of the average. Preferred orientation was investigated but it was found to be of little impact on the measurement and on the data analysis because the reflected intensity was essentially the same in the three measurement directions. This and the preferred orientation data indicate that the reflecting grains belong to the isotropically oriented fraction of the grains. Sheet metal textures due to rolling do not change significantly the elastic constants in the directions of the principal axis [14]. With the fact that aluminum is mechanically rather isotropic, this also allows the use of diffraction elastic constants calculated according to a self consistent scheme

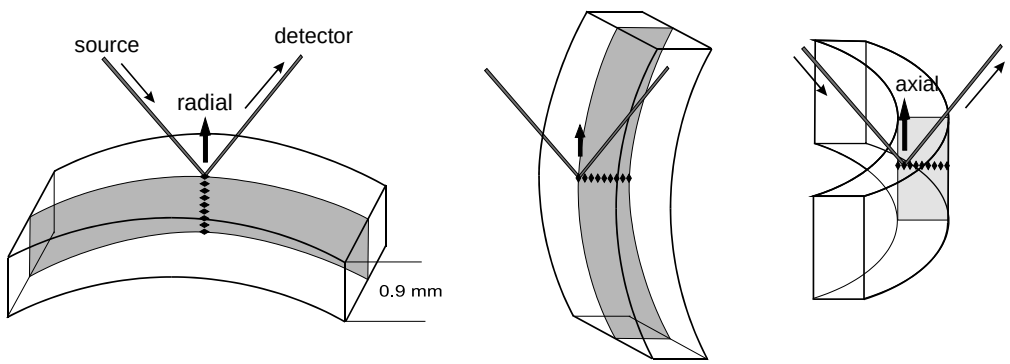

Fig. 2. Specimen orientations for the three principal strains.

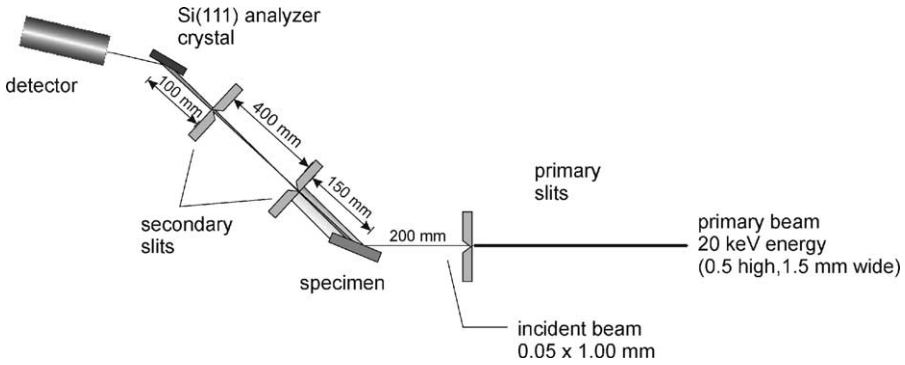

Fig. 3. Experimental arrangement of the synchrotron experiment. The incident beam penetrating the sample is diffracted along the entire path through the sample. The reflected beam is broadened due to microstrains in the sample. The low angular acceptance of the analyzer prevents the counting of photons that were reflected from regions outside the nominal sampling volume.

[11,12]. The stresses are obtained from the basic equation of diffractive stress analysis

$$\varepsilon_{\varphi\psi} = \frac{d_{\varphi\psi} - d_0}{d_0} = \tfrac{1}{2}s_2(hkl) \times [(\sigma_{11}\cos^2\varphi + \sigma_{22}\sin^2\varphi + \sigma_{12}\sin 2\varphi)\sin^2\psi + (\sigma_{13}\cos\varphi + \sigma_{23}\sin\varphi)\sin 2\psi + \sigma_{33}\cos^2\psi] + s_1(hkl)(\sigma_{11} + \sigma_{22} + \sigma_{33}) \quad (1)$$

By setting all shear stress components and σ_{33} equal to 0, one finds that

$$\varepsilon_{0,90} - \varepsilon_{0,0} = \frac{d_{0,90} - d_{0,0}}{d_0} = \tfrac{1}{2}s_2(hkl)\sigma_{11} \quad (2)$$

and

$$\varepsilon_{90,90} - \varepsilon_{0,0} = \frac{d_{90,90} - d_{0,0}}{d_0} = \tfrac{1}{2}s_2(hkl)\sigma_{22} \quad (3)$$

Using $\sigma_{11} = \sigma_{\text{axial}}$ and $\sigma_{22} = \sigma_{\text{tangential}}$, $d_{0,90} = d_{\text{axial}}$, $d_{0,0} = d_{\text{radial}}$, and $d_{90,90} = d_{\text{tangential}}$, we obtain for the stresses

$$\sigma_{\text{tangential}} = \frac{d_{\text{tangential}} - d_{\text{radial}}}{d_0} \times \frac{1}{1/2s_2(hkl)} \quad (4)$$

$$\sigma_{\text{axial}} = \frac{d_{\text{axial}} - d_{\text{radial}}}{d_0} \times \frac{1}{1/2s_2(hkl)} \quad (5)$$

For the diffraction elastic constant $1/2s_2(hkl)$ we calculated $1.9096 \times 10^{-5}\,\text{MPa}^{-1}$ [11]. The value of d_0 was estimated from the average of all measured d-spacings. It can be seen in Eqs. (4) and (5) that the uncertainty of this estimate for d_0 (approximately 10^{-5}) has no impact on the stress uncertainties (typically ±5 MPa).

3. Results and discussion

We collected data from 10 different positions through the wall. The experimental uncertainties are plotted in the graphs but they are in most cases of the size of the data points. The innermost and outermost locations were chosen

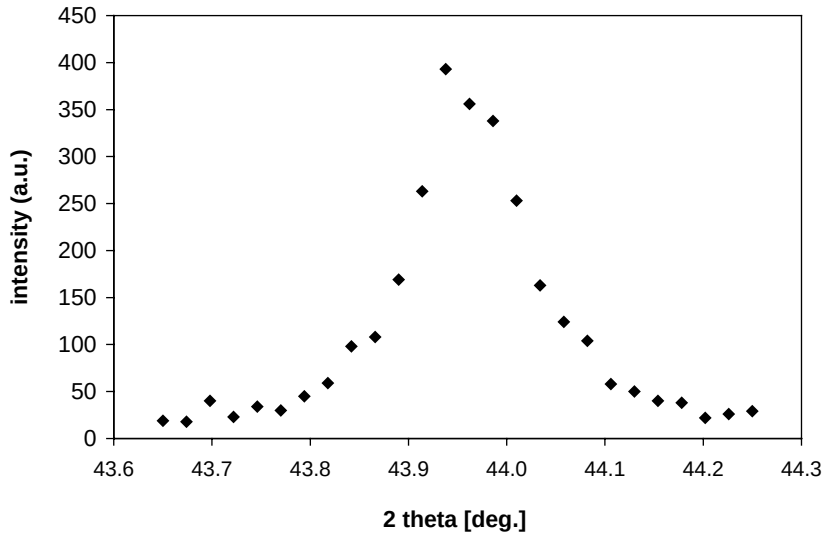

Fig. 4. Typical peak profile of the Al (4 2 2) reflection.

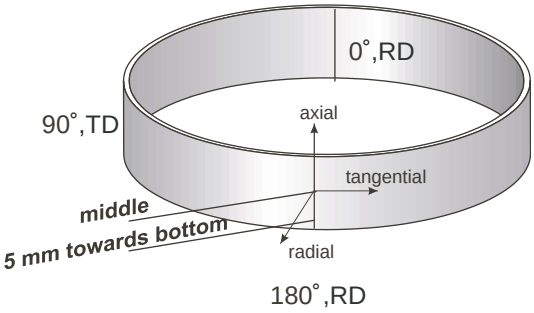

Fig. 5. Measurement locations on the ring. The axial direction is constant while the radial and tangential directions are rotated depending on the circumferential position: (a) 0° = RD; (b) 180° = RD.

such that the sampling volume was half immersed into the specimen. Due to the small beam size and the low acceptance angle of the analyzer/detector system, abberations that could affect the stresses at these two points are minimized. The use of laboratory X-rays for measurements directly at the surfaces was not considered because the stresses within the penetration depth ($\leq$10 μm) are affected by frictional surface damage [13]. While removal of the damaged surface layer with subsequent surface stress measurement is possible it would not add anything to the data because the new depths after removal are about the same as the depths (center of gravity) of the first (near the outer surface) and last (near the inner surface) sampling volume in our measurements. Also, unlike laboratory XRD, synchrotron radiation allows the direct measurement of in-plane strains (axial and tangential). For medium strength textures in rolled and deep drawn materials, the differences of elastic constants in the three measurement directions (principal axis system of the sheet) can be neglected [14], thus avoiding the difficulties involved in dealing with out-of-plane diffraction elastic constants as it is necessary for laboratory XRD [11].

3.1. Intact ring

We have investigated the depth distribution of axial and tangential stresses at two axial and two positions around the circumference for which the geometry is shown in Fig. 5. The tangential stresses were measured at the "0°" position and at the "180°" position, both of which correspond to the original rolling direction of the blank. The plots are shown in Fig. 6. The agreement between stresses at "0°" and "180°" is very good as was expected from the initial sheet symmetry. Circumferential coordinate measurement machine (CMM) scans of the wall thickness show that the thickness alternates similar to a sine wave with a 180° period and a maximum thickness difference between maximum and minimum of about 3%; however, this appears to be too small a variation to cause a difference in the stresses at both positions [15]. Similar CMM measurements on other cups have shown that the positions of the thickness minima and maxima are not correlated with the rolling direction or transverse direction (TD) [15]. The initial symmetry of the blank is given by rolling direction and transverse direction, thus suggesting a 90° period; the complete absence of this symmetry is a clear indication for an asymmetric material flow during the cup forming caused by an inhomogeneous blankholder force or variation from centering the blank (a misalignment of the die can be excluded). Compared to this combined effect the initial plastic anisotropy (due to preferred orientation) of the blank has a negligible impact on the cup wall thickness.

The change of the tangential stresses with the axial position has been pointed out in the literature [3,5,6], in this case we find a difference of appoximately 50 MPa over an axial distance of 5 mm, increasing from the mid-line towards the cup bottom. Because of the axial gradient there will be also a slight twist of the ring, i.e. both sides of the split ring will not align. As pointed out by Saito and Shimahashi [3], the origin of these stresses is the combination of a bending of the sheet metal at the radius of the die and the subsequent unbending at the radius of the punch. The intact ring is not in the tangentially unloaded state and the stress distribution is analogous to that of a plastically bent beam in a loaded configuration. Stress balance is neither demanded nor given for any of the individual curves of the tangential stresses. However, the equilibrium condition $\int \sigma_t \, dA = 0$ demands that the integral of the tangential stresses over the wall cross section of the ring vanishes. By extrapolating the stresses in Fig. 6 over the full wall cross section, i.e. by assuming that the tangential stresses at 5 mm up from the ring middle can be obtained by linear extrapolation it becomes clear that the equilibrium is not fulfilled which means that the variation of tangential stresses is non-linear in the axial direction. The through-thickness axial stresses, on the other hand, show little change in the axial direction (Fig. 7).

The comparison of the axial stresses in the ring middle and 5 mm down shows a gradient of about 5 MPa/mm decrease towards the bottom. Otherwise, the stresses in the ring middle both at the "0°" and at the "180°" mark are almost identical as was the case for the tangential stresses, thus confirming the accuracy of the data. The axial stresses show a similar behavior as the tangential stresses but they are well balanced with the resulting axial bending moment ≈0. This is a consequence of cutting the ring from the cup bottom (Fig. 1), thus setting the axial bending moment to zero *everywhere* in the ring.

3.2. Split ring

Splitting the ring partially releases the tangential stresses and it also resets the total tangential bending moment to zero.

The splitting is analogous to an unloading in the example of a plastically bent beam shown schematically in Fig. 8. Fig. 9 shows the axial and tangential stress distributions measured on the split ring. None of the individual through-thickness stress curves necessarily have a

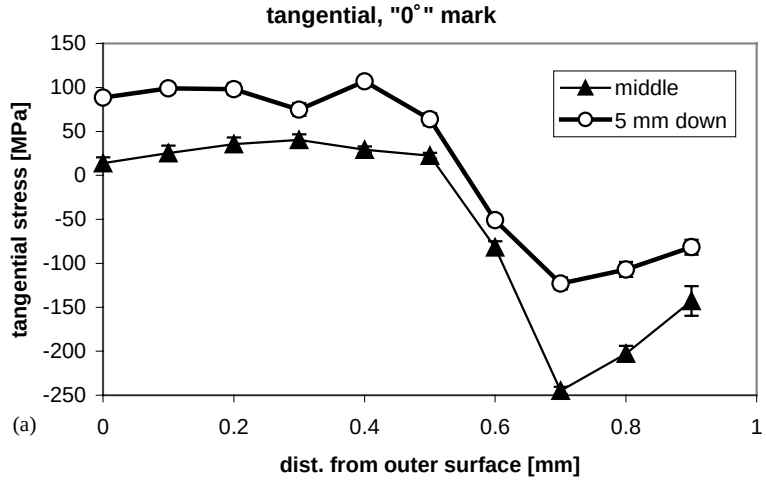

Fig. 6. Tangential stresses in the intact ring for the initial rolling direction. For an explanation of the labels see Fig. 4.

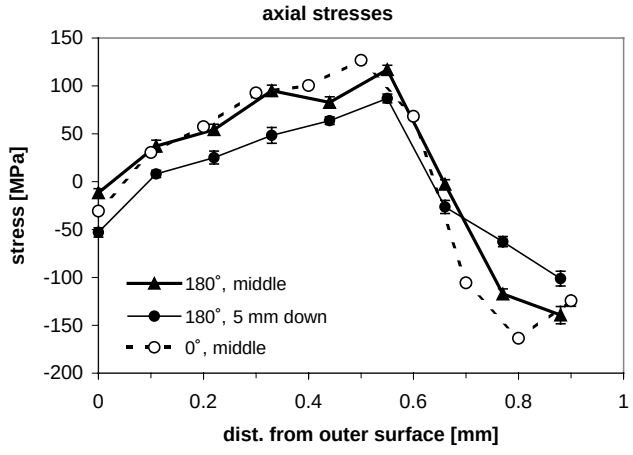

Fig. 7. Comparison of axial stresses: (a) loaded configuration; (b) stress change upon unloading; (c) residual stresses.

zero tangential bending moment (Fig. 9a); however, at a fixed angle (circumferential position) it must be true for the through-thickness tangential stress averaged over the width of the ring.

Unfortunately the synchrotron measurements could not be fully completed which is why the data at the "180°" mark were not taken at the same axial position as the others. Nonetheless, the tangential stresses all show the same behavior and the depth curve taken at "180°" is different from the ones at "90°" only by a small constant shift which means that there are only minor stress differences between locations at the RD and at the TD. The axial stresses are close to being identical. Significant changes with respect to the intact ring are found only for the tangential stresses which now exhibit the typical "S"-curve shape as shown in Fig. 8c. The direct comparison of stresses in the intact and split ring in Fig. 10 supports the interpretation given above.

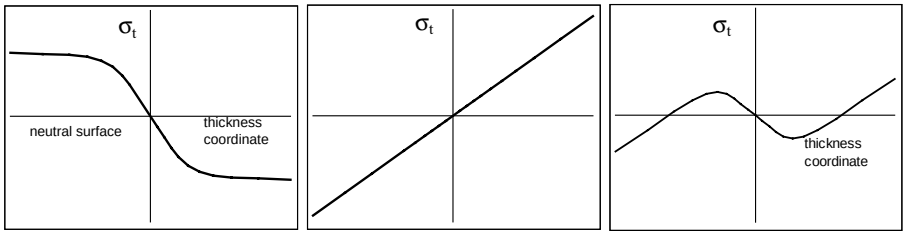

(a) loaded configuration (b) stress change upon unloading (c) residual stresses

Fig. 8. Stress distributions in elastic-plastic beam bending. Outer and inner surfaces have a negative and positive thickness coordinates: (a) tangential stresses; (b) axial stresses, respectively.

3.3. Springback

By averaging the measured tangential stresses from all locations we can estimate the total tangential stress change from the intact ring to the split ring which is shown in Fig. 11.

Using the intercept from the linear regression result in Fig. 11 we can calculate the curvature of the split ring. The equations needed are obtained as follows. First we calculate the new radius of the split ring from actual data of ring openings. An analysis of flatbed scanner images of split rings (accuracy ±0.05 mm) confirmed that the outline of the split ring is circular within ±1%, and the new radius R is obtained from the ring opening $2y$, the arc length c, and the old radius R_0 by means of two equations

$$c = 2R \arcsin\left(\frac{y}{R}\right)$$
$$c = 2\pi(R - R_0) \tag{6}$$

which have to be solved for R numerically. The meaning of the variables in Eq. (6) is shown in Fig. 12.

The linear stress change shown in Fig. 11 is associated with the change in curvature by

$$\sigma_t = E\varepsilon_t \tag{7}$$

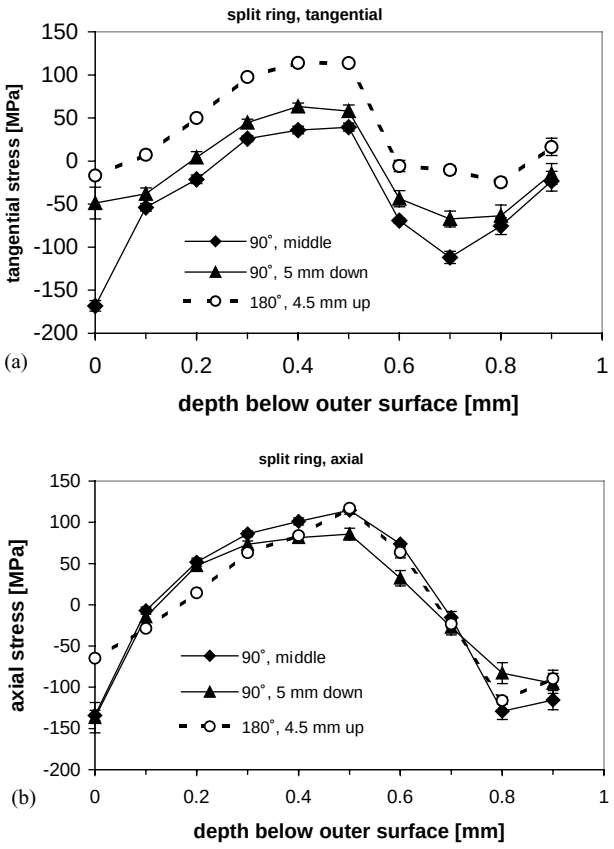

Fig. 9. Tangential and axial stresses in the split ring: (a) tangential stresses; (b) axial stresses.

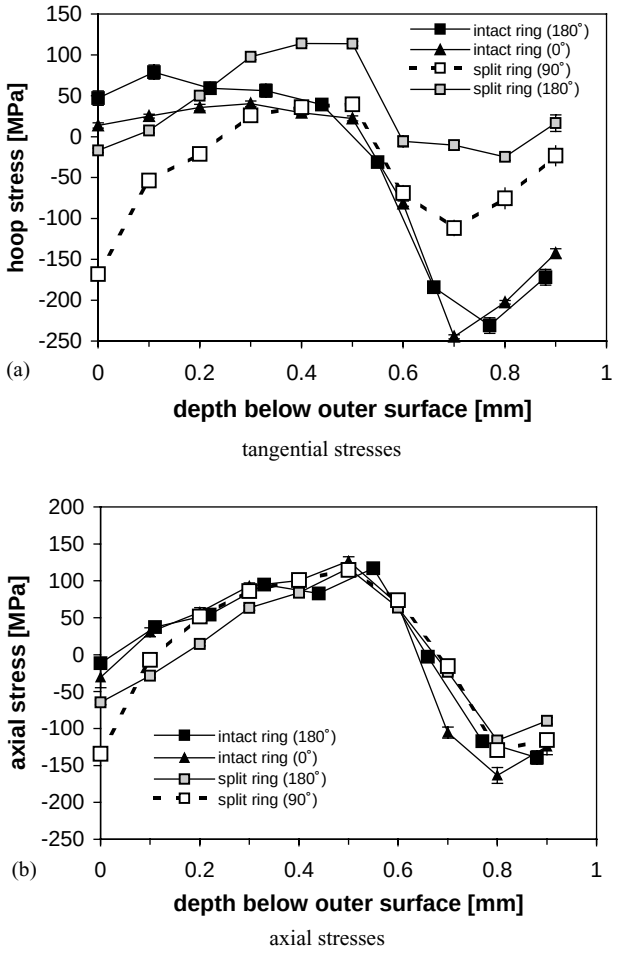

Fig. 10. Comparison of stresses in the split and intact ring.

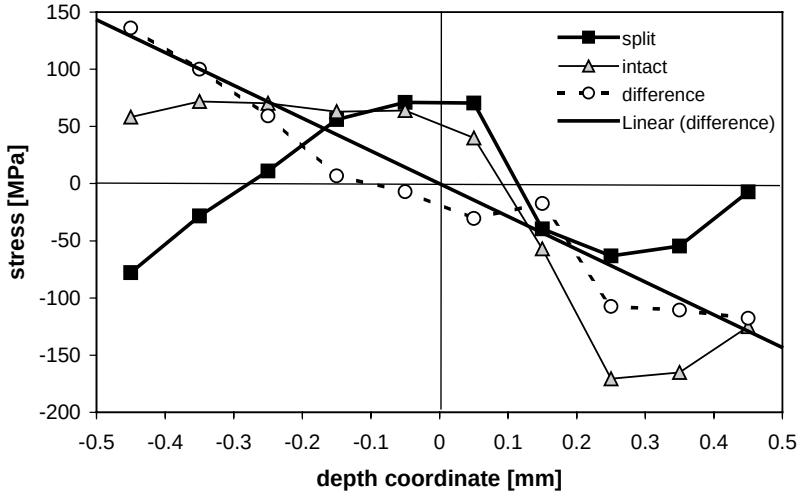

Fig. 11. Average tangential stresses in the intact and split ring as well as the difference between them plotted. The linear regression line is the average stress change from the loaded configuration to the unloaded configuration.

in which σ_t is the stress on the outer surface (this is the intercept in Fig. 11 with 130 MPa at $y = -0.46$ mm). For the bulk value of Young's modulus E a value of 70 GPa was used. The strain ε_t can be written in terms of the thickness d and the two radii R and R_0 as

$$\varepsilon_t = \frac{d}{2}\left(\frac{1}{R_0} - \frac{1}{R}\right) \tag{8}$$

from which R can be easily calculated. The results of the calculation and openings of several rings made under the same conditions are listed in Table 1.

The agreement between the calculated radius and the experimental results is good with a relative difference of just 3%. Keeping in mind that diffraction can inherently measure only *elastic* strains we find that within the accuracy of the measurement (the standard error of the intercept is 8%) there is no indication of plastic recovery which would appear as a difference between the calculated radius (purely elastic, calculated from through-thickness stress) and the measured radius of the split ring. The latter contains both the elastic effect and the plastic recovery.

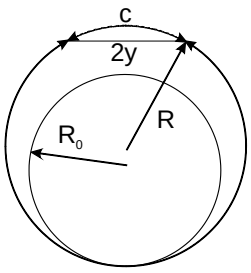

Fig. 12. Intact and split ring with radii R_0 and R.

3.4. Peak shape analysis

In addition to the shifts in position diffraction peaks also contain information about grain size and dislocation densities. These contribute to the full-width at half-maximum (FWHM) of a peak. The actual FWHM is a convolution of instrumental broadening and physical line broadening. One of the advantages of synchrotron radiation when used with an analyzer crystal is that for cold worked metals the contribution of the instrumental broadening is small compared to the physical line width. Because of that, changes in the FWHM can be tracked with high precision, as is shown in Fig. 13.

As shown by Wilkens [16], the line width increases with the dislocation density and inversely with domain size, and each effect has a different contribution depending on the diffraction angle. Our measurements are based on a single peak at a particular diffraction angle so that the domain size and dislocation contributions cannot be separated without additional information. However, a measure of grain size is available in the intensity fluctuations of the diffraction peaks in the axial and tangential configurations in which the absorption is constant for all locations. The two main contributing factors to the intensity fluctuations are the photon counting statistics and fluctuations of the diffraction grain volume from one position of the sampling volume to the next (under identical absorption conditions). The sampling volume is determined by the beam dimensions and it is constant. At different locations, the total volume of the grains within the sampling volume that contribute to the diffracted intensity varies depending on how many grains have the right orientation to meet the diffraction condition. Because of the high base intensity we can disregard the influence of the counting statistics (which would become apparent when measuring repeatedly at the same location under the same

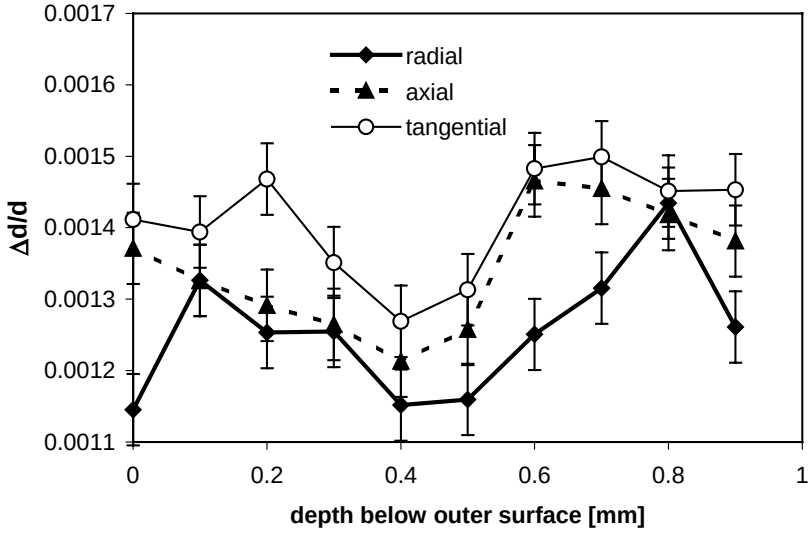

Fig. 13. Normalized FWHM for all three directions. Each individual curve is the average of all measurements at different axial or circumferential positions in the respective direction.

conditions) in which the relative standard deviation is <4%. For example, at one location the integrated intensity may be 1200(35) while at the neighboring location the integrated intensity is 800(28). The values in brackets indicate the standard deviation given by the counting statistics. Clearly, the difference between both intensities is far outside these limits. Thus, these large fluctuations are produced by variations of the diffracting grain volume.

In the following, a simple method to estimate grain dimensions is utilized. For a constant specimen orientation but different through-thickness locations, the standard deviations of the intensities are a measure of how much the diffracting volume varies from location to location. By disregarding preferred orientation and by assuming that the number of grains per sampling volume is Poisson-distributed, we obtain for n, the average number of reflecting grains, that

$$n = \left(\frac{E(I)}{\sigma}\right)^2 \tag{9}$$

in which $E(I)$ is the expectation value of the intensity and σ is the standard deviation of the intensity. $E(I)$ and σ are obtained from the intensities of through-thickness measurements at a given circumferential position. It can be assumed that no through-thickness texture gradients are left after the forming process. Using Eq. (9) we find for the axial orientation that $\sigma/E(I) = 0.33$ (relative standard deviation), and the number of relecting grains is $n = 9$; in the tangential orientation we obtain $n = 3$ with $\sigma/E(I) = 0.62$.

The different n in the two orientations indicate elongated grains. It is important to note that these numbers are independent of the multiplicity of the reflection (*hkl*). Furthermore, by assuming a uniform grain size and using the detector coverage (1.2×10^{-5} of the sphere determined by the sample to detector distance) together with the sampling volume of $3 \times 10^6\ \mu m^3$ we calculate the size of the diffracting volume to be $36\ \mu m^3$ (for an isotropic orientation distribution). We obtain an average grain volume of $12\ \mu m^3$ in the tangential orientation and an average grain volume of $4\ \mu m^3$ in the axial orientation. Even with large grain aspect ratios commonly found in rolled materials (approximately 520) these grain volumes point to grain sizes that will not contribute to a size broadening of the diffraction peak. As a consequence, the observed broadening effects are only due to dislocation related microstrains. Thus, the data in Fig. 13 are a measure of the accumulated plastic strain, distributed in symmetric curves with a minimum at the location of the neutral surface at 0.46 mm depth. The existence of the minumum is a consequence of the existence of a neutral plane in the sequence of bending and unbending.

4. Conclusions

The through-thickness residual stress distributions in a ring cut from a deep drawn Al-6022 cup in the loaded and unloaded state were measured non-destructively using synchrotron radiation. The measurements were performed with high spatial resolution and small step width in order not to lose details of the steep stress gradients in a wall <1 mm thick.

The tangential stresses both in the loaded (intact ring) and in the unloaded (split ring) state were measured at several locations and were found to be largely identical except for a constant shift. This shift depends mostly on the axial position and only to a small extent on the circumferential position, i.e. the position with respect to the original rolling direction. The axial stresses also showed some dependence on the axial position with a smaller constant shift than the tangential stresses. Unloading (splitting the ring) had only a small effect on the axial stresses.

A simple model was developed by which the opening of the split ring could be predicted from the stresses measured in the intact ring. The measured radius of the split ring was found to be within 3% of the calculated one.

References

[1] R.M. Cleveland, A.K. Ghosh, Int. J. Plast. 18 (2002) 769.
[2] J. Danckert, Ann. Int. Inst. Prod. Eng. Res. (CIRP) 43 (1994) 249.
[3] K. Saito, Y. Shimahashi, in: H. Lippman (Ed.), Proceedings of the Conference on Metal Forming Plasticity on August 1978, Tutzing, Germany, Springer, Berlin, 1979, p. 53.
[4] K. Lange, L. Bruckner, Trans. NAMRI/SME (1990) 71.
[5] Y. Yuying, L. Chunfeng, X. Hongzhi, J. Mater. Proc. Technol. 30 (1992) 167.
[6] M.S. Ragab, H.Z. Orban, J. Mater. Proc. Technol. 99 (2000) 54.
[7] F. Morestin, M. Boivin, C. Silva, J. Mater. Proc. Technol. 56 (1996) 619.
[8] T. Gnaeupel-Herold, T.J. Foecke, H.J. Prask, R.J. Fields, in: Proceedings of the TMS 2003 Annual Meeting, Mater. Sci. Eng. A, in press.
[9] H. Möller, G. Martin, K.W.I. Mitt, Eisenforsch. 21 (1939) 261.
[10] T. Gnäupel-Herold, H.J. Prask, in: Proceedings of the Sixth International Conference on Residual Stresses (ICRS-6), Oxford, UK, IOM Communications, London, 2000, p. 243.
[11] V. Hauk (Ed.), Structural and Residual Stress Analysis by Nondestructive Methods, Elsevier, Amsterdam, 1997, p. 132ff.
[12] E. Kröner, Zeitschr. Physik 151 (1958) 504.
[13] G. Petzow, Metallographic Etching, ASM Int., Materials Park, OH, 1999.
[14] U.F. Kocks, C.N. Tomé, H.-R. Wenk, Texture and Anisotropy, Cambridge University Press, Cambridge, UK, 1998.
[15] T. Foecke, T. Gnaeupel-Herold, Met. Mater. Trans. A (2003), in press.
[16] M. Wilkens, J. Appl. Cryst. 8 (1975) 191.